

Novel Polymer/Permanent magnet composites for bonding and advances 3D-Printing technologies

Nadia Alejandra Jiménez Olalla

Máster en Nanociencia
y Nanotecnología Molecular



MÁSTERES
DE LA UAM
2017 - 2018

Facultad de Ciencias

NOVEL POLYMER/PERMANENT MAGNET COMPOSITES FOR BONDING AND ADVANCED 3D-PRINTING TECHNOLOGIES

Nadia Alejandra Jiménez Olalla



FACULTAD DE
CIENCIAS

Director: Dr. Alberto Bollero
Tutor: Dr. Julio Camarero de Diego
Lugar de realización: IMDEA Nanociencia (Madrid)
IMA S.L. (Ripollet)

Trabajo de Fin de Máster. Curso 2017-2018

AUTORSHIP STATEMENT

Me, **Nadia Alejandra Jimenez Olalla**, with **72897297Q** NIF, student of the master on Nanoscience and Nanotechnology from the Faculty of Science from *Universidad Autónoma de Madrid*, related to the Master Thesis presented to be evaluated in the year **2017-2018**, I declare that I assume the originality of this project, and no sources were used without their appropriate references.

Madrid, September 3rd 2018

Signature:

ACKNOWLEDGEMENTS

This work was supported by the Spanish Ministerio de Economía y Competitividad (MINECO) through:

- NEXMAG project [M-era.Net Programme, Ref. PCIN- 2015-126]. Coordinator: Dr. A. Bollero
- 3D-MAGNETOH project [Ref. MAT2017-89960-R]. Coordinator: Dr. A. Bollero/Dr. E. M. Palmero

And by the following industrial collaboration:

- "Plastic Magnets". IMA S.L. (Barcelona) and IMDEA Nanociencia (PI: Dr. A. Bollero).

TABLE OF CONTENTS

ACKNOWLEDGEMENTS	2
1. ABSTRACT	4
2. INTRODUCTION	4
2.1 MAGNETIC PROPERTIES	5
2.2 PERMANENT MAGNETS	6
2.3 MAGNETIC DOMAINS	7
2.4 HYSTERESIS	7
2.5 DEMAGNETIZATION	9
3. RARE-EARTH CRISIS	10
4. BONDING TECHNOLOGY	12
5. EXTRUSION OF BONDED MAGNETS. PRINCIPLES AND PROCEDURE. ..	12
6. BASES OF BONDING FOR 3D-PRINTING	13
7. LABORATORY EQUIPMENT	15
8. FERRITE STRIPS	17
8.1 MAGNETIC PROPERTIES	17
8.2 HOMOGENEITY STUDIES	19
a) CUMULATIVE DISTRIBUTION FUNCTION (CDF)	19
b) STUDENT T-TEST	20
9. REDUCTION OF RE MATERIALS ON PERMANENT MAGNETS	20
9.1 HYBRID BONDED SAMPLES	20
9.2 EXPERIMENTAL DETAILS	21
a) EXTRUSION PROCESS	22
b) EXPERIMENTAL ANALYSIS	22
10. CONCLUSIONS	25
BIBLIOGRAPHY	26
ANNEX	27

1. ABSTRACT

Nowadays, the technological growth is following an exponential trend in terms of power and performance. Rare Earth based permanent magnets are a crucial component of these development, however their access is being restricted by the main supplier, China. Therefore, alternatives must be found for avoiding geopolitical dependences and development difficulties. This project is included in the alternative of reduction of RE in permanent magnets using bonding technology. Furthermore, its application in 3D-printing opens the possibility of overcoming design and manufacturing restriction for the creation of high-performance permanent magnets with no limitation in shape and dimensions, from which could be benefitted the energy, automotive and aerospace sectors.

Keywords: bonding technology, 3D-printing, reduction of rare earth in permanent magnets, hybrid permanent magnets.

2. INTRODUCTION

Magnetism and magnetic fields were one of the oldest, but at the same time oddest, physical phenomena investigated and subjected to measurements. Since the time of ancient Chinese between 300 and 200 b.C, there are evidences of the use of loadstones to create compasses because of its capability to point North direction [1].

Since then, discoveries have been slow but with an imperious relevance.

Charles-Augustin de Coulomb (1736-1806) formulated *Coulomb's law* describing mathematically the force F between hypothetical magnetic poles m_1, m_2 distanced by r as

$$F = \frac{1}{4\pi\mu_0} \frac{m_1 \cdot m_2}{r^2} \quad (1)$$

The magnetic field (B in eq. 2) tries to align the magnetic dipole M parallel to direction of this field with torque τ

$$\tau = M \times B \quad (2)$$

In 1820, Jean-Baptiste Biot and Felix Savart along with Ampère's contributions proposed the *Biot-Savart law*, that determines that the magnetic field strength H generated by a current I in a circuit C of a conductor at a radial length a is

$$H = \frac{1}{4\pi} I \int_C \frac{dl \times u}{a^2} \quad (3)$$

Actually both models were referring the same, the most elementary entity in magnetism: the magnetic moment m which is defined as two magnetic poles of opposite polarity, separated by some distance (fig. 1-1)

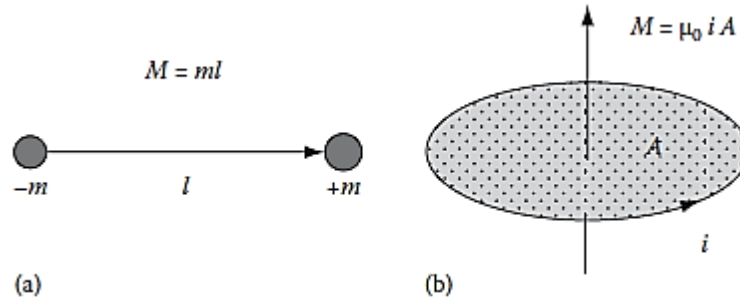


Figure 1-1: (a) magnetic moment proposed by Coulomb. (b) Circular circuit where the current creates a magnetic moment perpendicular to the section of the coil proposed by Ampère [1].

Later, in 1831, Michael Faraday discovered another fundamental law of magnetism: the *electromagnetic induction (EM)*, where a magnetic flux Φ linking an electrical circuit changes, it induces in this circuit electromotive force (voltage V) proportional to the rate of change of the flux:

$$V = -\frac{d\Phi}{dt} \quad (4)$$

The minus indicates that the voltage generated is opposite to the flux that generates it (*Lenz's law*).

To finish, it is compulsory to state the four main equations from James Clerk Maxwell of the electromagnetism which are fundamental to any analysis in magnetism:

$$\nabla \cdot E = \frac{\rho_v}{\epsilon} \quad (5)$$

$$\nabla \cdot H = 0 \quad (6)$$

$$\nabla \times E = -\mu \frac{\partial H}{\partial t} \quad (7)$$

$$\nabla \times H = J - \epsilon \frac{\partial E}{\partial t} \quad (8)$$

2.1 MAGNETIC PROPERTIES

A magnetic field describes a volume of space where there is a change in energy. As Ampère suggested, a magnetic field is produced whenever an electrical charge is in motion. The direction of the spin and orbit determine the direction of the magnetic field. It is denoted by \vec{H} , and gives rise to a magnetic induction given by \vec{B} .

$$\vec{B} = \mu_0 \mu_r \vec{H} \quad (9)$$

$$\mu = \mu_0 \mu_r \quad (10)$$

Where μ_0 is the permeability in vacuum, μ_r corresponds to the relative permeability of an specific material and μ is the total permeability of the medium that comprises both contributions. Theoretically, μ_r could be the best factor for describing the properties of magnetic materials because it shows how is affected a material by an external magnetic field. However, the permeability is usually a tensor dependent on other parameters as the operation point of the magnet, the direction of magnetization, the presence of harmonics

and more [1]. Therefore, although permeability may be a very useful factor, in technical applications it is more useful to apply the magnetization curve, that will be explained hereafter.

The magnetization is the sum of all the magnetic moments contained in a volume of material:

$$\vec{M} = \frac{\sum_i \vec{m}_i}{V} \quad (11)$$

When a material is placed in an external magnetic field, the applied field tends to align the dipoles from the magnetic moments. The relation between both magnitudes is called *susceptibility* χ ,

$$\chi = \frac{M}{H} \quad (12)$$

χ changes when increasing the field strength, until a moment when remains constant. That means that the material cannot undergo further progress within that field and reaches the saturation.

It is important to note that χ is a bulk property so does not depend on the shape, alike μ . Both are related through the expression,

$$\mu = \mu_0(1 + \chi) \quad (13)$$

Depending on their magnetic response, bulk materials can be classified through their susceptibility upon an external magnetic field. Within this project, we will be talking about those materials with positive, large χ , because they successfully response to an external input saturating all their magnetic moments, and, even more, are able to retain this magnetization after removing the external field. Those materials are called *permanent magnets*.

2.2 PERMANENT MAGNETS

Permanent magnets are a special case because they are not passive against a magnetic field, but can actively act as a magnetic source due to their capability of retention the internal magnetization. For that reason, there are some considerations to take into account when describing them.

Going back to equation (9), it has to be included an internal contribution from the magnetized material $\mu_0\vec{M}$ to the effect of the external magnetic field $\mu_0\vec{H}$, leading to a corrected expression

$$\vec{B} = \mu_0(\vec{H} + \vec{M}) \quad (14)$$

The magnetic induction B , usually called magnetic flux density, has been widely used for describing magnetic materials. Nevertheless, recently many standards have shifted their notation into the *magnetic polarization* J , what is the intrinsic flux density given by:

$$\vec{J} = \vec{B} - \mu_0\vec{H} \quad (15)$$

So, polarization \vec{J} is equal to $\mu_0\vec{M}$.

2.3 MAGNETIC DOMAINS

The magnetic moments \vec{m}_i comprised in a material are arranged in subgroups with the same orientation. These groups are referred as magnetic domains. The sum of the contribution of all vectors \vec{m}_i give raise to a net magnetization in the bulk material. When the magnetic domains are randomly oriented, cancelling each other, the material is demagnetized. If an external field is applied, the domains begin to turn parallel to it, until a moment where all of them are set in the same direction, saying that the material has reached its maximum magnetization, the saturation magnetization. Before this state, two domains are not necessarily parallel, but are separated by a domain wall, which is a transition region of approx. 100 nm where the magnetization rotates gradually (fig. 1-2).

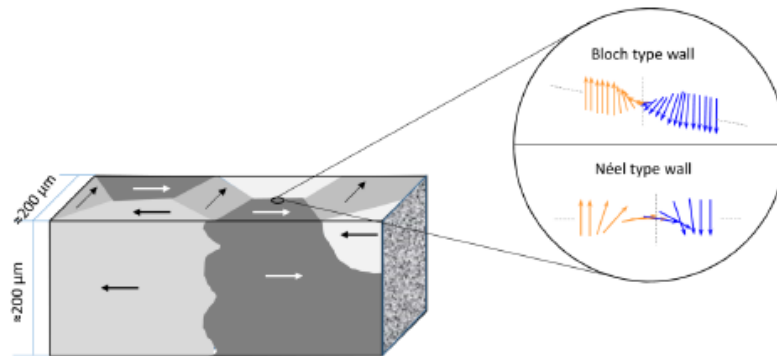


Figure 1-2: magnetic domains and domain walls. Extracted from [2].

The evolution of the magnetic domains upon a magnetic field is also dependent on other factors, as would be magnetic anisotropies. Due to the internal atomic structure of the material, there are certain directions that are easier to magnetize than others, because they are energetically favourable.

Magnetocrystalline anisotropy arises from dipole-dipole interactions and spin-orbit coupling. But there are many others that contribute to the total anisotropy, as the shape anisotropy (magnetostatic) and the stress anisotropy (magnetostriction) [3].

2.4 HYSTERESIS

A hysteresis loop is the evolution of a magnetic feature of the material upon an external magnetic field sweep, like $M(H)$, $B(H)$, $J(H)$, $\mu(H)$. Per se, a hysteresis loop is the path that follows a feature depending on the history of the material [4].

A ferromagnetic material, originally demagnetized, starts to increase its magnetization upon a magnetic strength until reaching the saturation M_s . This first curve is called the virgin curve (point 1 to 3 in fig. 1-3). Afterwards, when removing the applied field, the magnetization remains and the value when $H_{ext} = 0$ is called *remanence magnetization* M_r . When applying a negative magnetic field, M starts lowering, until a moment where all the magnetic domains are randomly oriented cancelling their total net magnetization. The field required to reverse it (point 4 to 5) is the coercivity field H_c . Eventually, if the magnetic strength keeps increasing in the negative direction, it will reversely saturate (point 6), coming back to the beginning (point 3) through a symmetric path.

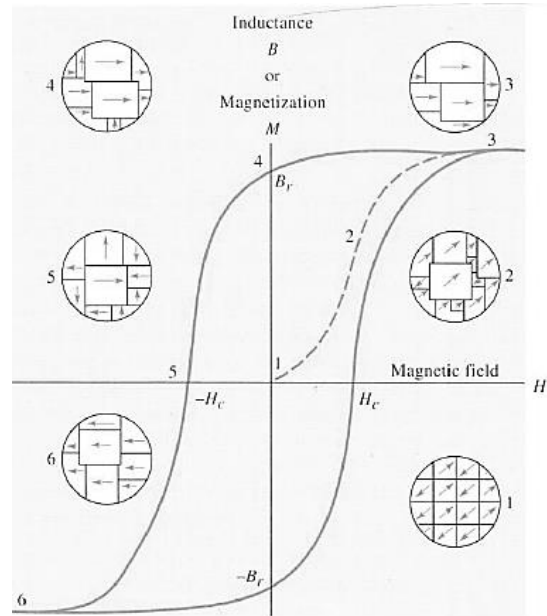


Figure 1-3: Hysteresis loop $M(H)$ from a ferromagnetic material [4].

The permeability μ_r correspond with the slope B/H and the configuration of magnetic domains in each stage are indicated in the insets. The region of highest permeability is governed by domain wall motion whereas magnetization rotation occurs rather at higher magnetic fields.

It is also possible to display the hysteresis loops through $J(H)$ and $B(H)$, called the intrinsic and the normal loop, respectively (fig. 1-4).

For describing a ferromagnet, three are the most relevant magnitudes: J_r (or B_r), H_{cj} (or H_{cb}) and $|BH|_{max}$. H_{cj} (sometimes just called H_c), being the required field to demagnetize a material, distinguishes from *hard magnets* to those who have large coercivity, and *soft magnets* to those which are easily demagnetized and possess low H_{cj} .

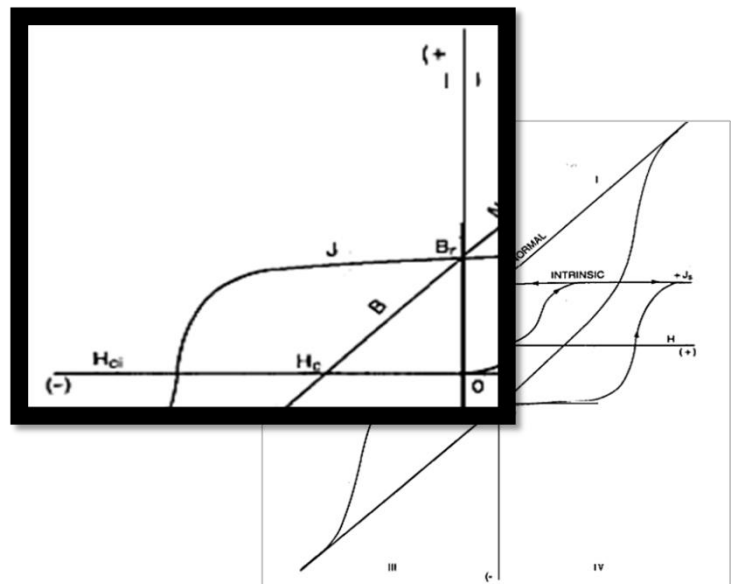


Figure 1-4: Normal $B(H)$ and intrinsic $J(H)$ hysteresis loops. Zoom inset of the second quadrant [5].

The $(BH)_{max}$ value is the most important figure of merit to describe the quality of a permanent magnet, called maximum energy product. It is the area under the curve from the second quadrant of the $B(H)$ loop, because it provides a measure of the magnetic energy density that can be stored in the considered material. For that reason, the main aim is to enhance this area. Unlike M_r and H_{cj} , the energy product (BH) is an extrinsic feature that can change with the shape and size of the magnet. It can take values from every point of the second quadrant of the $B(H)$ curve, that are usually referred as working points for a specific shape. The $(BH)_{max}$ is just the point where lies the design able to store the maximum energy density, as is depicted in fig. 1-5.

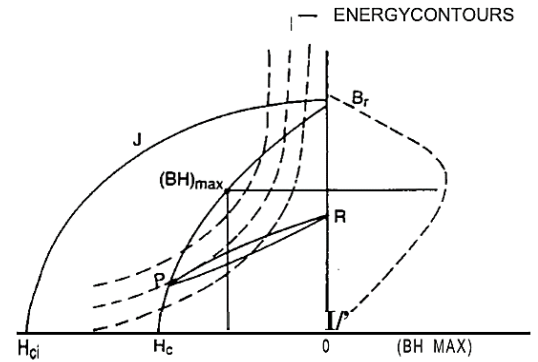


Figure 1-5: Values of (BH) related to each working point [5].

2.5 DEMAGNETIZATION

When a permanent magnet is removed from the magnetizer, free poles are established and a field potential $-H_d$ (demagnetizing field) exists between both poles. It is a potential due to some of the internal magnetization J that tries to oppose the external field (fig. 1-6).

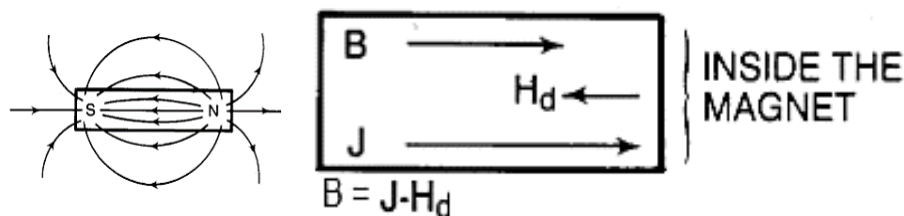


Figure 1-6: Scheme of the free poles generated in a magnet that generate a demagnetization field [5].

The field H inside the magnet at any point is the result of the applied field and the demagnetizing field. Therefore, $H = H_{ext} + H_d = H_{ext} - NJ$, where N is the demagnetization factor. In closed magnetic circuit H_d will be zero since the free poles do not exist. For a magnet in an open circuit or for a magnet circuit containing an air gap the effect of H_d will be to lower the magnetization J . N is geometrically dependent and its values are tabulated. At the end, its interest falls in the variation of the working point and the performance of the magnet.

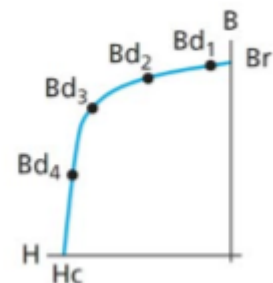


Figure 1-7: Shift of the operating point depending on permeance [6].

The higher the field lines H leaving the magnet through the poles, the larger H_d and the lower B , because the flux in the magnet is no longer passing through the magnet to the close circuit, but leaking to the sides. The resulting relation between B/H is called *permeance* and determines where the working point falls in the second quadrant (noted as Bd_x in fig. 1-7).

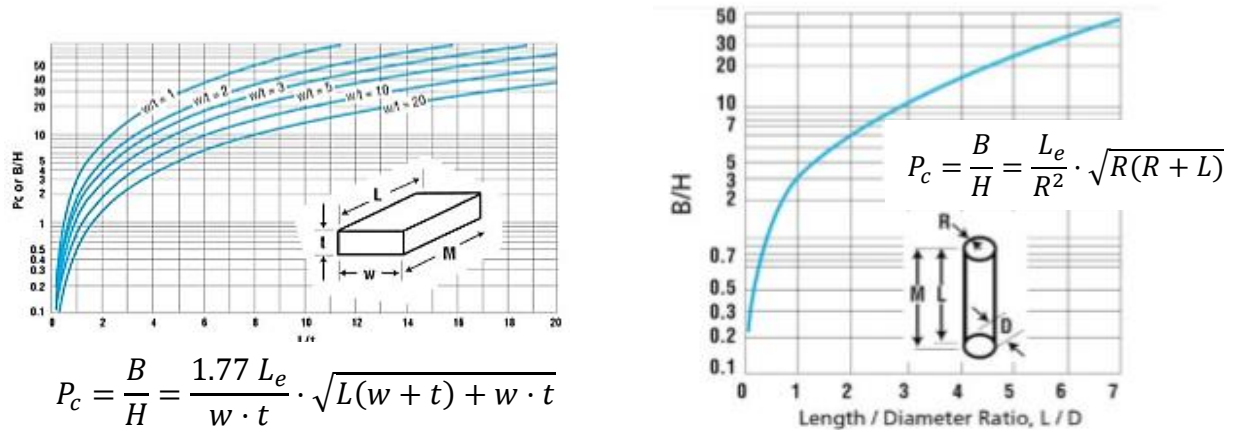


Figure 1-8: (left) Permeance coefficient B/H dependence to dimensions of a rectangular prism of ferrite or Rare Earth magnet. (right) Permeance coefficient B/H dependence to dimensions of a cylinder of ferrite or Rare Earth magnet [6].

The permeance analysis represented in fig. 1-8 has a particular relevance for designs dealt to applications as holders or sensors, as might be magnetic strips (left) or magnetic filaments (right).

The working point changes whenever magnets move relative to each other, when the air gap changes or when time-varying currents are present.

From the distinction of magnets by means of the evolution of the second quadrant of the normal loop (fig. 1-4) it is possible to classify them as: linear, when the link between B_r and H_{cb} is straight; non-linear (fig. 1-7), when a “knee” exists within this line; and quasi-linear if it is in between.

The harder is a magnet the more linear it is, what is a crucial aspect in design. When a material is non-linear, a subtle shift of the working point can drastically change the energy product that is being obtained from the magnet, contrary to those materials which have a linear relation. For instance, NdFeB is considered linear, while hard ferrites are quasi-linear.

3. RARE-EARTH CRISIS

As noted above, in an ideal permanent magnet, a large remanent magnetic flux B_r must be maintained in the absence of a magnetic field and be matched with a large resistance

to demagnetization (intrinsic coercivity H_{cj}). Hereby, it will be possible to strengthen the maximum energy product $/BH/_{max}$ [7].

Materials that can be easily magnetized and exhibit large permeability are some of the 3d transition metals (iron, cobalt and nickel). In metals, strong coupling between atoms in the crystal lattice exists due to the close proximity from one to another. As a result, the band structure representing the energy levels between 3d and 4s orbitals is split up and because of Pauli exclusion principle, many energy levels are hold only by one electron, leading to a large magnetic moment (fig 2-1)

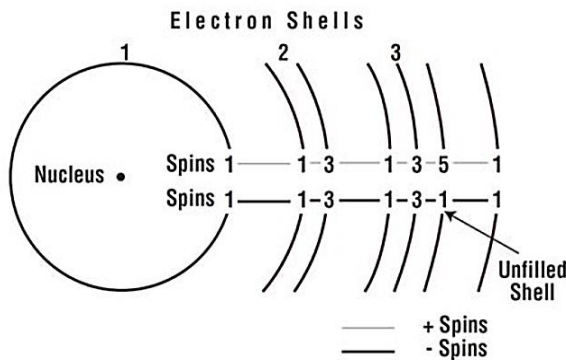


Figure 2-1: Electron shells in an atom of iron [6].

In the other hand, the extremely strong magnetocrystalline anisotropy field H_k provided by the rare earth 4f electrons boosted by local interatomic environment surrounding a magnetic atom, increase the magnetic field necessary to demagnetize the material, i.e. H_{cj} .

In the mid-1960s, at the University of Dayton, Ohio, they took the advantage of these two groups to create the reign of the rare-earth “superparamagnets”. Strnat’s team of researchers reported high energy products in ferromagnetic intermetallic phases of the type $RE(TM)_5$ with space group $P6/mmm$. Here RE is a rare-earth element or mixture, in particular containing Y, Ce, Pr, Sm, and (TM) is a transition metal, namely Fe, Co or Ni. Continued exploration of the rare-earth/transition metal alloys resulted in the introduction in 1972 of a new rare-earth-based intermetallic compound $RE_2(TM)_{17}$, where TM was mainly cobalt. But due to political instabilities in the region of Zaire, the global supply of cobalt was jeopardized greatly increasing its cost. It was the birth of a new iron-based supermagnet, $Nd_2Fe_{14}B$, whose space group is $P4_2/mnm$, being able to get up to energy products of 50 MGOe (400 kJ/m^3) [7].

This brought a groundbreaking prospect to the technology, being able to provide large torques and high strength with no need of other sources. Furthermore, the fast development of the technology that aims to boost the power while reducing in size is making imperative the use of those that are capable to produce high energy density in small space. Hard disks, wind turbines and hybrid cars are just some examples benefited from this technology.

The danger began in 2011 with the “rare-earth crisis”. Since September, China which currently produces 95% of the world supply, decided to limit the exportation worldwide or, even, stop it. Other mines, as in the north of Australia, have been reopened, however not only the limited capacity of those new mines entails a problem but their extraction comes

along with radioactive elements [8]. This situation has brought an imperative necessity of finding alternatives for rare-earth free permanent magnets or, at least, permanent magnets with reduced RE content. It seems another revolution is about to come as happened with the instabilities of cobalt supply. In my group at IMDEA Nanoscience we are working in those two lines, and my project is included in the reduction of RE content using the bonding technology and later implementation in 3D-printing.

4. BONDING TECHNOLOGY

Permanent magnets are often classified into sintered and bonded magnets.

Sintered magnets are made by the pulverization into fine powder, compaction and heat to cause densification via “liquid phase sintering”. On the other hand, plastic-bonded magnets are particle composites with permanent- magnet powder embedded in a plastic binder. For embedding the magnetic particles, thermoplastics binders as, for instance, polyamide (PA), polyphenyl sulfide (PPS), styrenics as acrylonitrile butadiene styrene (ABS) or copolymers as ethylene acrylic acid (EEA) are used. Although bonded materials are inferior in terms of magnetic performance in comparison with sintered (as result of reduction of magnetic part in the whole volume), they present many other advantages:

- Exhibit excellent mechanical properties (depending on the binder type)
- The non-magnetic binder lowers the density of the magnet and dilutes the contribution of the magnetic powder.
- Show excellent geometric tolerances with minimal or no secondary operations.
- Enable to create more complex shapes.
- Present higher electrical resistivity.
- Allow multipole magnetization, enhancing magnetic force.
- Minimize eddy current losses.

5. EXTRUSION OF BONDED MAGNETS. PRINCIPLES AND PROCEDURE.

There are four main processing routes used to manufacture the majority of bonded magnets. These processes are injection moulding, extrusion, calendaring and compression bonding.

Until now, injection and compression have been the most used methods for bonded magnets manufacturing [9]. However, this project is based mainly in the refinement of the extrusion process of composite materials combining magnetic particles embedded in a polymeric matrix that might be included in an *Additive Manufacturing (AM) process*. This method is attracting much interest for the development of functional structures dealt to a broad of applications in sectors such as automotive, energy and aeronautics [10]. It is capable of building objects from computer-aided designs models by adding layer-by-layer of material. Some of the advantages over conventional subtractive manufacturing

processes are: minimum waste and energy usage, less processing time, no additional tooling costs, no size and shape limitations.

In contrast to the other three techniques which obtain final products, extrusion of bonded magnets may be used for generating feeding materials for another technique, like filaments in 3D-printing, or end-products like magnetic strips. Nevertheless, there is an innovative technique that covers all the steps in one. It is called *Big Area Additive Manufacturing (BAAM)* and might become a revolution in terms of industrial manufacturing [11].

The feeding material of the extruder are pellets made of a controlled mixture of polymer and magnetic powder, made up through solution casting process. It is possible to use commercial pellets with specific composition or synthesize using the solution casting method. For this purpose, firstly the polymer is dissolved using a suitable solvent. Afterwards, the powder is added and mechanically stirred to avoid particles agglomeration. Finally, the residual solvent is evaporated leading to a solid composite that might be broken up into pellets [12].

In short, the extrusion screw works against a heated barrel to push the composite pellets through a heated die at high pressure (fig. 4-1). The resulting extruded material is then collected in a spool prepared for further steps. It should be noted that magnetic materials are very abrasive what may increase the temperature at the nozzle and make the process more complicated.

Depending on the material composition and production process, isotropic and anisotropic composites are employed. Anisotropic composites are much more expensive; however, their performance is remarkably improved from their counterparts. This is not always helpful. Indeed, isotropic materials are more commonly used in bonded magnets, while anisotropic are the vast majority of sintered magnets.

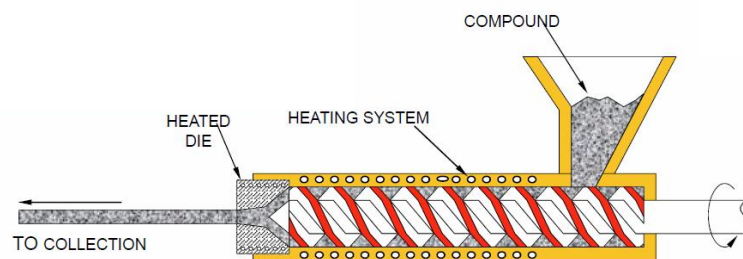


Figure 4-1: Extruder scheme.

6. BASES OF BONDING FOR 3D-PRINTING

Additive manufacturing (AM) enables the translation of computer-aided designs (CAD) virtual 3D models into physical objects. By digital slicing of CAD, 3D scan, or tomography data, AM builds objects layer by layer without the need for moulds or

machining. Furthermore, AM allows decentralized fabrication of customized objects on demand by exploiting digital information storage and retrieval via Internet.

The scientific and technological impact of AM has steadily increased since the first commercial instruments were introduced in the late 1980s. At this time, better known as “rapid prototyping”, the economical motivation was to accelerate and lower the costs related to product development. Research publications have exponentially grown with favourable expectations in fields as aerospace, energy, automotive, consumer products and medical/ dental.

AM includes 3D-printing technique. Herein, I will highlight fused deposition modelling (FDM) inside extrusion-based AM, because it appears as an interesting technique for advanced 3D-printing of magnetic materials. Mainly consists in the computer controlled layer by layer deposition of molten and semimolten polymers, pastes, polymer-based solutions through a movable nozzle or orifice serving as the extrusion print head (fig. 5-1(left)). After completing a single layer, either the extrusion head moves up or the build platform moves down to allow the deposition of the next layer. FDM comprises 3D extrusion of thermoplastic polymers, which are mechanically fed as thin filaments from a spool into the extrusion print head. The extruder is heated to an appropriate process temperature for the amorphous polymers.

FDM filaments for feeding the printer are produced as stated in section 4. For a particular filament, a careful balance of polymer melt rheology, processing temperature, build speed, CAD shape parameters, filling index, filling pattern and support material are essential for a successful build process.

Regarding polymers, thermoplastics are suitable for FDM. The most prominent ones are acrylonitrile-butadiene-styrene copolymers (ABS), polylactide (PLA), polycarbonate (PC) and polyamides (PA).

Although, FDM has been only considered a flexible technology platform for printing of plastic components, my group in IMDEA Nanoscience is taking a stand in the development of 3D-printed permanent magnets [10], even with free RE-permanent magnets [12].

For that purpose, we used 1.75 mm diameter filament of our “home-made” composite material with different feedstock inserted in the 3D-printer shown in fig 5-1 (right). *Slicer.exe* was used for designs in .stl format.

Filaments created until now have been made of Sr-ferrite and neodymium (IMA S.L collaboration), MnAl(C) (Höganäs AB collaboration), first time reported in the literature, and steel and aluminium (RAMEM S.A collaboration). The binder has mainly been ABS and PE, however another successful tries were done with EEA.

Whereas FDM is based principally on polymer crystallization and chain entanglement limited to extrusion of thermoplastics at elevated temperature, other techniques enable many other classes of materials including thermosets, rubbers, polyurethanes, silicones as 3D micro extrusion, 3D dispensing etc. Depending on the application, those might be the target for future studies on magnetism.

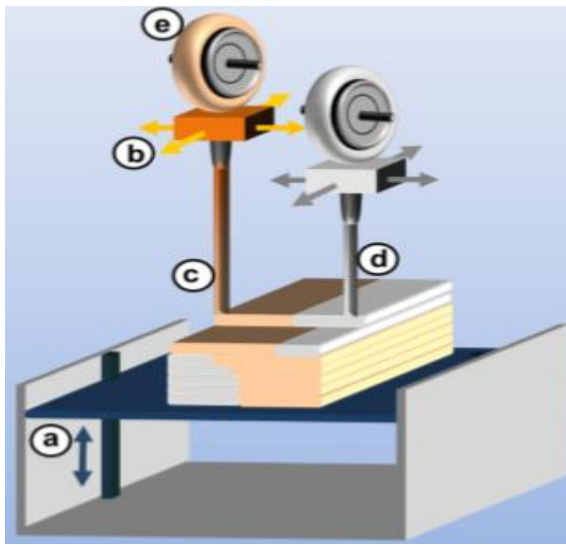


Figure 5-1: (left) Fused deposition modelling process invented by Scott Crump, comprised by a movable vertical platform (a) and two tempered extrusion printing heads for model (c) and support (d) feeding material contained on a feedstock spool (e). Both heads are allowed to move in XYZ (b) [13]. (right) Real example of 3D printer for FDM.

7. LABORATORY EQUIPMENT

For the analysis of the magnetic properties of the samples three main machines were used. Firstly, my group at IMDEA Nanoscience is provided with a vectorial vibrating sample magnetometer (v-VSM) with possibility of applying a maximum magnetic field of 3T (fig. 6-1). This technique allows measuring the most intrinsic property of a ferromagnet with high precision and sensitivity. VSM is based on Faraday's law which states that an electromagnetic force is generated in a coil when there is a change in the flux through the coil [14]

In the measurement setup, a magnetic sample vibrates in the proximity of two pick-up coils. This oscillation provides a sinusoidal signal that is translated by the transducer assembly into a vertical vibration. It is centered between the two pole pieces of an electromagnet that generates a magnetic field \vec{H}_0 of high homogeneity. The symmetry of the pickup coils coincides with the magnetic center of the static sample. Hence, the change in magnetic flux originated from the vertical movement of the magnetized sample induces a voltage U_{ind} in the coils.

$$U_{ind} = -\frac{\partial\Phi}{\partial t} \quad (16)$$

Where Φ is the magnetic flux that is expressed as the magnetic flux B density that crosses a section A :

$$\Phi = B \cdot A \quad (17)$$

At the end, the induction voltage detected by the pick-up coils is produced by the variation of flux density created by a magnetized sample vibrating the z-direction. The resulting induction voltage is

$$U_{ind}(t) = -\frac{3\hat{z}}{4\pi} \cdot m \cdot \mu_0 \cdot \cos(\omega t) \cdot \sum n_c \cdot \sum n_w \int_A d\vec{A} \cdot \left(\frac{1}{r^7}\right) \cdot \mathbf{G}. \quad (18)$$

It is dependent on some parameters as the frequency ω of the vibration and its amplitude \hat{z} , the magnetic moment of the sample m and the distance. Furthermore, the number of windings n_w and the number of pick up coils n_c may increase the signal reading by the machine. As a result, the VSM is able to detect the signal of sample up to nanograms.

Furthermore, in transient mode, performing magnetic field sweeps we can obtain the hysteresis loop of our sample that provides the most important magnetic parameters [2].

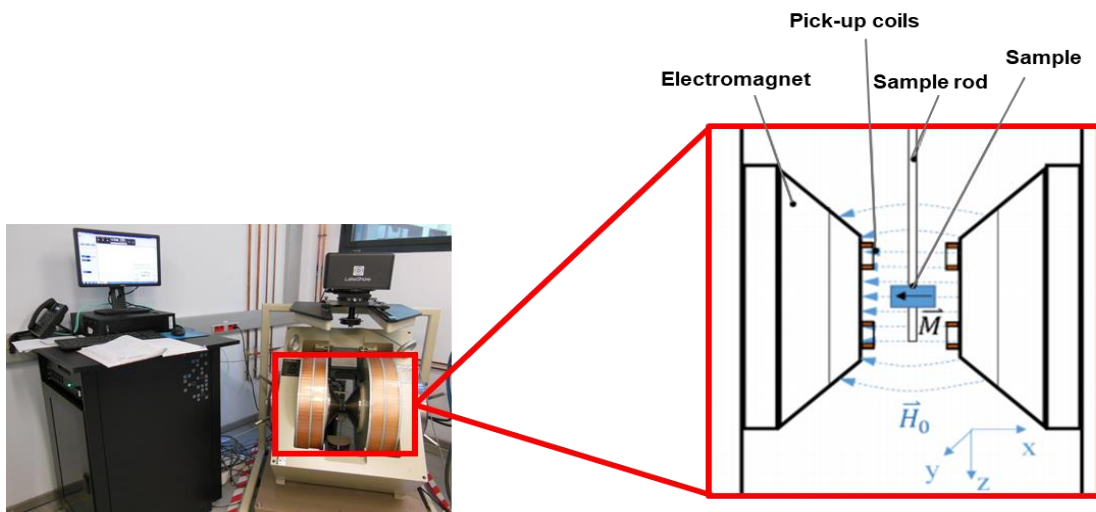


Figure 6-1: Vectorial vibrating simple magnetometer (v-VSM) at IMDEA Nanoscience. Scheme extracted from [2].

Secondly, at IMA S.L. laboratory the equipment available was a (a) permagraph (fig.6-2(a)) and (b) fluxometer (fig. 6-2 (b))

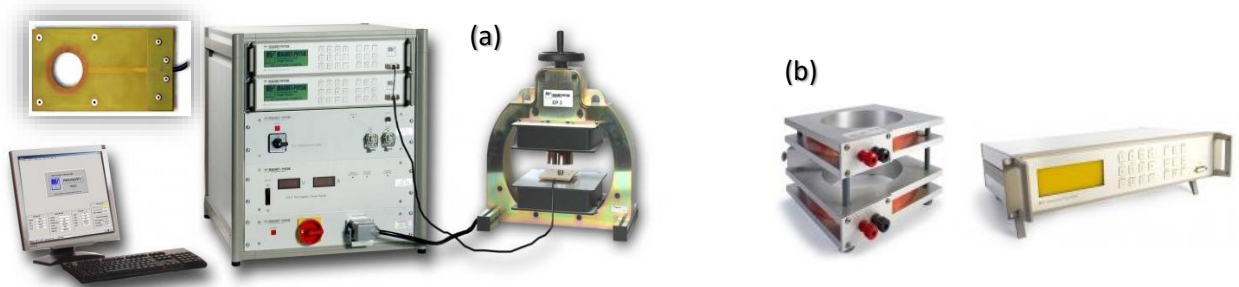


Figure 6-2: (a) Permagraph-C from Magnet-Physik, comprised by electromagnet, fluxometers, surrounding coils and a computer-aided system for collecting data. (b) Fluxometer and Helmholtz coil (moment coil) from Magnet-Physik.

Unlike VSM, those techniques are not as sensitive and precise, but are sufficient for bulk measurements. Normal and intrinsic curves were taken in close circuit mode with a permagraph (a) provided with two H and J fluxometers and surrounding coils of different sizes. For performing the experiments, the source provided the current that created the external magnetic field at the electromagnets (up to 1700 kA/m or 2.1T). The detection was carried out by the surrounding coils, where the sample is introduced and all together are closed inside the yokes.

In the other hand, for faster measures a Helmholtz coil and a J -fluxometer were used. It applies the same operation principles as the previous one, but in a passive mode, because the fluxometer reads the voltage created in the coils due to the flux density emitted by an already-magnetized sample.

8. FERRITE STRIPS

In the next section extruded bonded ferrites will be analyzed in terms of magnetic performance and homogeneity through the extrusion process, ensuring their reliability under operation.

Those strips were extruded at IMA S.L. using an *Xcalibur* Noztek model and commercial pellets compounded by 92 wt% of Sr-Ferrite ($\text{SrFe}_{12}\text{O}_{19}$) and 8 wt% of EEA (ethyl ethylene acrylate).

Among the applications of those strips are included the use as pop-up display system, magnetic labelling, door gaskets, retail display etc. All of them are used in stationary mode.

Due to measuring equipment limitation, only 15 mm width – 2 mm height strips were analyzed. Further experiments, varying size will be done.

For the analysis, two bunches of fifty samples for each strip were tested. Each bunch was die-casted on a rolling basis, avoiding space between them for a more reliable assessment of the homogeneity.

8.1 MAGNETIC PROPERTIES

The first comparison consisted on the magnetic properties from the raw material (pellets), two different bunches of an oriented sample and another two different bunches for a non-oriented one.

The relative mean and standard deviation of the coercivity (H_{cj}), remanence (B_r) and maximum energy product ($/BH_{max}$) are graphically displayed in fig. 7-1 along with their numerical values collected in table 7.1

The main aim was getting the best of the starting material when analyzing the resulting strips, for that reason the relative values are plotted considering the raw material as the

maximum value of each feature. Although the relative standard deviation is represented, it is so tiny that it is not possible to perceive it in the graph.

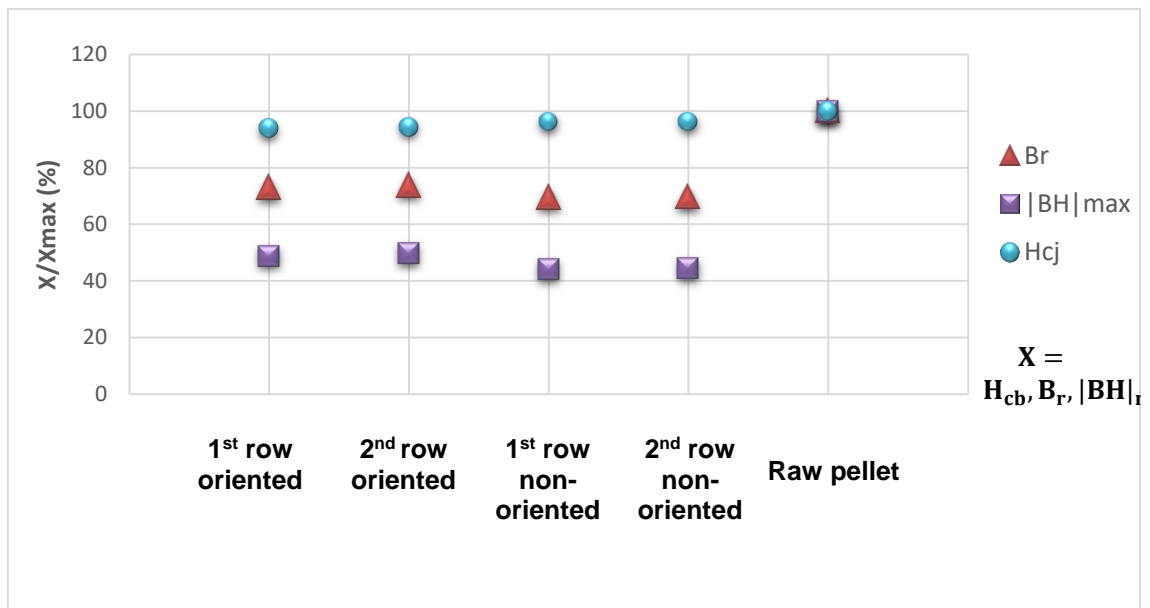


Figure 7-1: Relative magnetic values for the oriented and non-oriented strips along with the starting material.

Table 7.1: Values corresponded to fig 7-1

	H _{cj} (kA/m)	s (H _{cj})	B _r (T)	s (B _r)	BH _{max} (kJ/m ³)	s (BH _{max})
1st row ORIENTED STRIP	225	0.51	0.217	0.00144	8.3	0.112
2nd row ORIENTED STRIP	226	0.67	0.219	0.00145	8.5	0.107
1st row NON ORIENTED STRIP	231	0.29	0.206	0.00144	7.5	0.098
2nd row NON ORIENTED STRIP	231	0.28	0.207	0.00106	7.6	0.070
RAW PELLETT	240	-	0.297	-	17.0	-

In conclusion, during the extrusion the coercivity remains high, however the remanence lowers around 30%, what, as a result, decreases the maximum energy product around 50%. It is a preliminary result and further efforts will be done to improve it.

In second place, we were expecting bigger differences between the oriented and non-oriented strips, especially considering that we are dealing with an anisotropic starting material. Probably, the configuration of the nozzle is not enough to make a difference in the extruded product.

8.2 HOMOGENEITY STUDIES

In order to ensure the homogeneity or non-homogeneity of the strips, a double check analysis was carried out. As stated before, the target value was the $|BH|_{max}$ and both samples were tested separately.

a) CUMULATIVE DISTRIBUTION FUNCTION (CDF)

In probability theory and statistics, the cumulative distribution function of a real random variable X ($|BH|_{max}$) is the probability that X will take a value less than or equal to x . If the CDF F of a real valued random variable X is continuous, then X is a continuous random variable:

$$F(b) - F(a) = P(a < X \leq b) = \Phi(\mu, \sigma)(a < X \leq b)$$

Two assumptions have to be taken into account:

- As symmetric is the function, as more Gaussian behaviour adopts and more reliable will be.
- As vertical the function is, less distribution data will present.

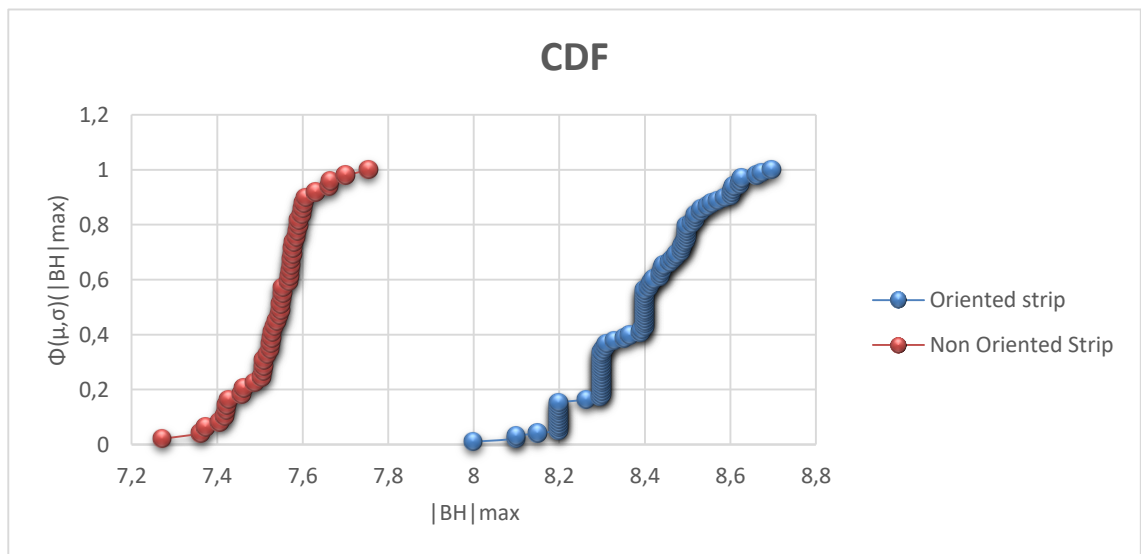


Figure 7-2: Cumulative distribution function for oriented and non-oriented strips

According to fig. 7-2, the non-oriented strip shows a quasi-vertical trend what suggests a good homogeneity, in contrast to the non-oriented one. However, those are not conclusive results

b) STUDENT T-TEST

The t-test is any statistical hypothesis test in which the test statistic follows a Student's t-distribution under the null hypothesis. The t-test can be used, for example, to determine if two sets of data are significantly different from each other. It is most commonly applied when the test statistic would follow a normal distribution.

In this study, two groups of samples from each strip are going to be compared to determine if they are significantly different. The imposed boundaries are that at 95% of confidence the values meet the hypothesis H_0 . H_0 is $\mu_a = \mu_b$, therefore the alternative hypothesis is that $\mu_a \neq \mu_b$.

An independent two-tailed is carried out through the analysis of a common standard deviation s_{ab} what allows the determination of the experimental t_{exp} .

$$s_{ab} = \sqrt{\frac{(n_a-1)s_a^2 + (n_b-1)s_b^2}{n_a+n_b-2}} \rightarrow t_{exp} = \frac{|\bar{x}_a - \bar{x}_b|}{s_{ab} \sqrt{\frac{1}{n_a} + \frac{1}{n_b}}}$$

The critical t values for each confidence level are already tabulated. When comparing the experimental values in the table, if $t_{exp} < t_{tabulated}$ then H_0 is accepted, otherwise is rejected. The results conclude that the non-oriented sample can be considered homogenous, however the oriented one does not.

9. REDUCTION OF RE MATERIALS ON PERMANENT MAGNETS

As it was previously said, there is an imperative necessity to reduce the amount of rare earth elements on permanent magnets for economic interests from the industrial point of view. Thus if we compare the price per kg of neodymium is around eighty times higher than ferrite price.

9.1 HYBRID BONDED SAMPLES

Contemporary research in the field of magnetic composite materials on the basis of Nd–Fe–B alloys are directed to reduction of the subtle rare earth content (Nd), targeting towards decreasing the price of the final magnetic material while keeping high values of the maximum magnetic energy.

The presented study is undertaken with intention to investigate the effect of different filler content on the structural and magnetic properties of the Nd–Fe–B/strontium ferrite hybrid composite materials in order to fulfill new technological demands while improving

economic yielding, because of the lowered manufactured costs (as no costly finishing is necessary) and decreased raw material prices.

9.2 EXPERIMENTAL DETAILS

Already bought pellets made of composite materials have been used for the mixtures. Two types of composite pellets were used: one of strontium ferrite, $\text{SrFe}_{12}\text{O}_{19}$ (fig. 8-1 (right)), and $\text{Nd}_2\text{Fe}_{14}\text{B}$ (fig. 8-1 (left)) powders, embedded into a polymeric matrix of ethylene ethyl acrylate (EEA) with binder content of 8 wt% and 6.6 wt%, from here referred as neo pellet and ferrite pellet respectively.

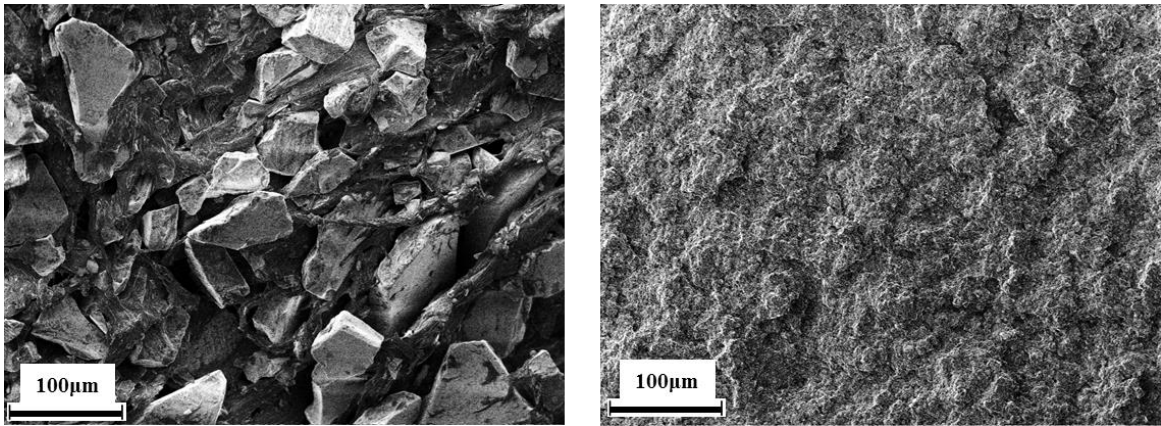


Figure 8-1: (left) SEM image $\text{Nd}_2\text{Fe}_{14}\text{B}$ -EEA pellet. (right) SEM image $\text{SrFe}_{12}\text{O}_{19}$ -EEA pellet.

Placing as goal the magnetization value, 100 % NdFeB bonded strip and 100 % ferrite strip were considered as the top and bottom extreme. Then 4 equidistant values were calculated for preparing the mixtures in table 8.1.

Taking into account that the raw materials differ on the density, the mass will not be the same as the proportion in the compound.

Table 8.1: Relative content of $\text{Nd}_2\text{Fe}_{14}\text{B}$ and $\text{SrFe}_{12}\text{O}_{19}$ for each hybrid bonded magnet based on a magnetization goal (grey). The mixtures were prepared from the percentage of mass colored in green.

	M ($\mu\text{Wb}\cdot\text{cm}$)	Vol Neo pellet(%)	Vol Ferrite pellet (%)	m Neo pellet (%)	m Ferrite pellet (%)	Neo pellet density
1	15.86	100	0	100	0	5.28 g/cm ³
2	13.69	80	20	85	15	Ferrite pellet density
3	11.52	60	40	68	32	3.76 g/cm ³
4	9.35	40	60	48	52	
5	7.18	20	80	26	74	
6	5.01	0	100	0	100	

a) EXTRUSION PROCESS

During the extrusion process takes place the merge of both magnetic powders since the pellets have not been generated in situ, but by an external supplier. It may imply a drawback for getting a homogeneous mixture and well combined magnetic properties. For that reason, the extrusion process must be very controlled and careful.

Individual sachets of 50 g. were prepared with each mixture in order to obtain at least five meters of strip, allowing the analysis at different stages. During the whole process the extruder was fed slowly, controlling that the proportion of each material entering was the same. The speed of the screw was set at 8 rpm and the temperature at the three stages was set at 95°C/95°C/90°C during the whole extrusion. Higher levels of temperature are required at the beginning of the screw (enabling the melting of the pellets), whereas reducing the temperature at the nozzle creates pressure that ensure a more successful finishing.

A second study was carried out. The strips were collected and die-casted in the desired shapes and sizes. Thereafter, the leftover material was restored, demolished as a pellet size and reincorporated into the extruder, in order to analyze the effect in the homogeneity and merging of the materials during the extrusion.

b) EXPERIMENTAL ANALYSIS

The main parameters of interest for the characterization of our extruded strips are the magnetization in open-circuit and the hysteresis loops in close circuit.

For simplicity, the analysis has been taken with samples of the same shape and size, avoiding dimensional dependences. All the samples were die-casted on cylinders of 2 ± 0.1 mm height and 14 ± 0.2 mm of diameter.

As said before, the criteria to set the mixing values was to achieve certain values of magnetization. Magnetization values for the first extrusion samples and restored samples were measured with the fluxometer in open-circuit. From here, the mean and standard deviation for 20 samples each are compared in table 8.2.

Firstly, regarding magnetization in open circuit, the experimental values do not considerably differ from the expected ones and the standard deviation represents less than 5% of the mean. The restored samples do not improve substantially, therefore it would not be considered a successful refinement process.

TABLE 8.2: magnetization values from first extrusion (1^a) and second extrusion from restored material and comparison to the expected values obtained with the fluxometer.

	M ($\mu\text{Wb}\cdot\text{cm}$)	M (1 ^a) ($\mu\text{Wb}\cdot\text{cm}$)	s	M (res) ($\mu\text{Wb}\cdot\text{cm}$)	s
1	15.86	-	-	-	-
2	13.69	13.30	0.227	13.40	0.223
3	11.52	11.20	0.280	11.00	0.348
4	9.35	9.53	0.198	9.31	0.063
5	7.18	8.80	0.290	8.28	0.293
6	5.01	-	-	-	-

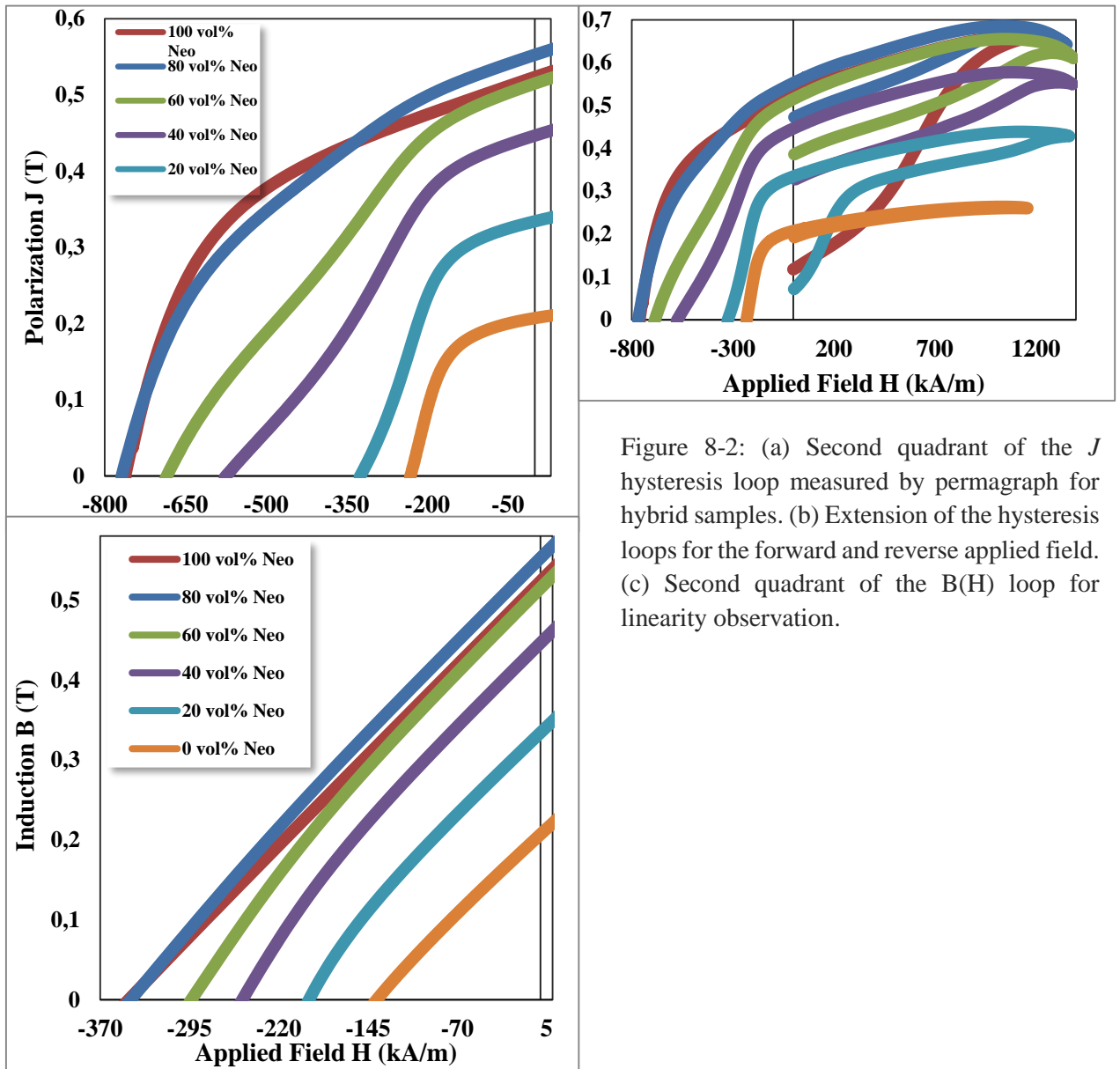


Figure 8-2: (a) Second quadrant of the J hysteresis loop measured by permagraph for hybrid samples. (b) Extension of the hysteresis loops for the forward and reverse applied field. (c) Second quadrant of the $B(H)$ loop for linearity observation.

TABLE 8.3: Main magnetic parameters in both measuring systems SI and CGS obtained with permagraph.

	Units in SI			Units in CGS		
	Hcj (kA/m)	Br (T)	BH max (kJ/m ³)	Hc (kOe)	Mr (emu/g)	BH max (MGOe)
1	760	0.523	46	9.6	78.82	5.78
2	764	0.553	48	9.6	88.44	6.03
3	698	0.515	41	8.8	87.72	5.15
4	574	0.446	32	7.2	81.25	4.02
5	363	0.353	21	4.6	69.12	2.64
6	230	0.206	8	2.9	43.60	1.00

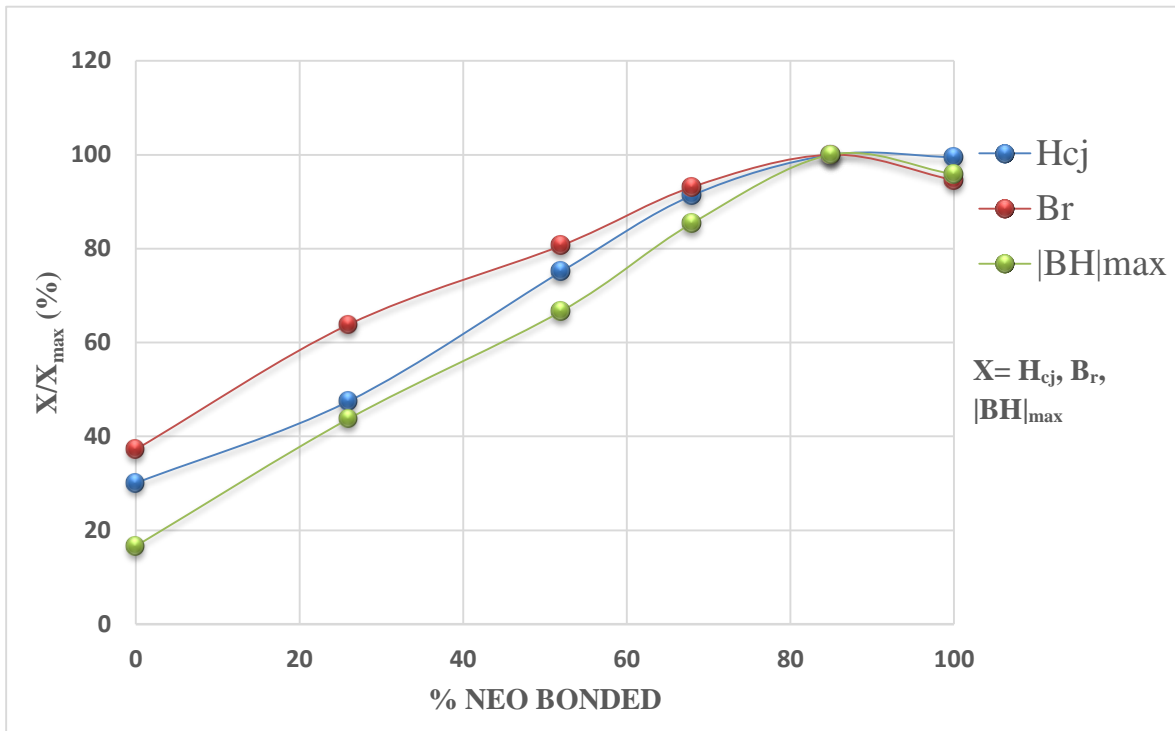


Figure 8-3: Dependence of the coercivity, remanence and maximum energy product on neodymium content.

The impact of increasing the content of neodymium in the mixture is plotted in the fig. 8-3. Both, H_{cj} and B_r increase when adding neodymium, although is B_r what makes a bigger difference on $|BH|_{max}$. The optimum value would be considered 85% Neodymium – 15% Ferrite, which is even better than pure neodymium bonded strip magnet, due to the higher B_r value.

Those results are quite promising when comparing with the limited research papers published to date about hybrid bonded magnets. [15] reported remanence values of 0.28 MGOe and [16] reached 1.60-1.7 MGOe, whereas [17] did not conclude positive results. Those remain far from the results submitted here for the strips with 85% Neodymium – 15% Ferrite, which reaches more than 7 MGOe of maximum energy product, 613 mT of remanence and 9.6 kOe of coercivity.

As is noted in [15]-[16], if we have a look to the second quadrant of the $J(H)$ loop in the fig. 8-2, the curves from the hybrid composites exhibit a “knee” what outlines a non-complete exchange between the materials. It has not the same impact if we attend to the $B(H)$ loop, where the curves present an almost linear behavior. However, that may impose a drawback in performance. Therefore magnets made of those materials would need an in-depth design, because there is not a flattering region as in hard magnets where the energy product does not drop drastically with a subtle increase of the strength field.

10. CONCLUSIONS

Within this project it is exhibited the forthcoming need of replacing rare earth-based materials in permanent magnets for avoiding geopolitical dependences, beside environmental issues which are increasingly causing worldwide concern. Until now, no alternatives have been discovered capable of exceeding or matching the strength found on RE-based permanent magnets, however, between transition metal and RE permanent magnets there is a gap of possibilities which many new technological applications could benefit from.

One interesting proposal is the reduction of RE content through bonding technology. Besides decreasing the magnetic content, bonded magnets offer good mechanical properties, avoid corrosion, minimize eddy currents, reduce secondary finishing operation and greatly reduce material costs. Furthermore, they can be included in an additive manufacturing process, often called 3D-printing technology, offering the possibility of creating magnets of shapes and sizes that have never built before, opening a new horizon in technological development.

Promising results have been obtained on hybrid bonded magnets compounded of $\text{SrFe}_{12}\text{O}_{19}$ and $\text{Nd}_2\text{Fe}_{14}\text{B}$ merged by EEA. The best result is attributed to the 85 wt% of neodymium pellet with 15 wt% ferrite pellet, reaching values even higher than 100 wt% neodymium pellet. This may be due to difficulties to extrude neodymium, whose particles are large and pointed, what might hinder the extrusion process. Moreover, the grainy ferrite particles can facilitate the way out (fig. 8-1). The strips have reached 9.60 kOe of coercivity, 5.53 kG of remanence and 6.03 MGOe of maximum energy product.

The results substantially exceed those from other researching groups. The best results from the competitors [16] are $B_r = 3.70$ kG, $H_c = 3.70$ kOe and $|\text{BH}|_{\text{max}} = 1.70$ MGOe mixing a weight ratio of $\text{BaO}_6\text{Fe}_2\text{O}_3$: Nd-Fe-B 70%/30% with 5% epoxy resin. In our case the composite based on the weight ratio of $\text{Nd}_2\text{Fe}_{14}\text{B}/\text{SrFe}_{12}\text{O}_{19}$ of 68%/32% with 7% of EEA features $B_r = 4.80$ kG, $H_c = 8.70$ kOe and $|\text{BH}|_{\text{max}} = 5.50$ MGOe.

Future steps will be:

1. Reconfigure the extruder nozzle via simulations for a more effective orientation of the material while extruding, improving then the performance of the material.
2. Applying those materials on 3D-printing, opening new opportunities on renewable energy, aerospace, automotion and other growing technologies.

BIBLIOGRAPHY

- [1] Tumanski, S. *Handbook of magnetic measurements*. Poland: CRC Press, 2011. Accessed
- [2] Alamdar, S. et al. *Vibrating Sample Magnetometry: Analysis and Construction*. Retrieved from Department of Physics, Syed Babar Ali School of Science and Engineering. LUMS, 2013.
- [3] *Chapter 4: Magnetic anisotropy and domains*. Retrieved from <http://ltauxe.github.io/Essentials-of-Paleomagnetism/WebBook3ch4.html>
- [4] Donald R., Pradeep P., Wendelin J. *The Science and Engineering of Materials*. Stamford: Cengage Learning, 2011. Accessed.
- [5] Mr. Parker from the Magnetic Materials Producers Association. *Permanent Magnet Guidelines*. Chicago: MMPA PMG-88, December 1988.
- [6] White, L. *Understanding Permanent Magnets Theory*. TECHNNotes **13(2)**, 1-2 (2008).
- [7] Lewis, L., Jiménez-Villacorta, F. *Perspectives on Permanent Magnetic Materials for Energy Conversion and Power Generation*. Metallurgical and Materials Transactions A **Vol 44A**, S(2-20), 2013 Jan.
- [8] Bourzac, K. *The rare-earth crisis*. Technology Review **114(3)**, 3-5 (2011).
- [9] Guo, N., Leu, M. *Additive manufacturing: Technology, applications and research needs*. Frontiers of Mechanical Engineering **8(3)**, 215-243 (2013)
- [10] E.M. Palmero, et al. *Magnetic Polymerized Composites for Bonding and 3D-Printing of Permanent Magnets*. IEEE.
- [11] Li, L., Tirado, A. et al. *Big Area Additive Manufacturing of High Performance Bonded NdFeB Magnets*. Scientific Reports **6**, 1-7 (2016).
- [12] E.M. Palmero, et al. *Development of permanent magnet MnAlC/polymer composites and flexible filament for bonding and 3D-printing technologies*. Sci. Technol. Adv. Mat. **19(1)**, 465 (2018).
- [13] S.C. Ligon et al. *Polymers for 3D Printing and Customized Additive Manufacturing*. Chemical reviews **117(15)**, 10212-10290 (2017).
- [14] Lake Shore Cryotronics, Inc. User's Manual 7300 Series VSM System. Retrieved from http://www.lakeshore.com/ObsoleteAndResearchDocs/7300_Manual.pdf, 2001.
- [15] N. Idayanti et al. *The implementation of hybrid bonded permanent magnet on permanent magnet generator for renewable energy power plants*. IEEE **978**, 557-560 (2016).
- [16] Muljadi et al. *Preparation and characterization of hybrid bonded magnet Ba-ferrite/NdFeB with epoxy resin*. Material Science Forum **864**, 65-69 (2016).
- [17] J. Schneider et al. *Bonded hybrid magnets*. Journal of magnetism and magnetic materials **157-158**, 27-28 (1996).

ANNEX

Units for Magnetic Properties

Symbol	Quantity	Conversion from Gaussian and cgs emu to SI
Φ	magnetic flux	$1 \text{ Mx} \rightarrow 10^{-8} \text{ Wb} = 10^{-8} \text{ V}\cdot\text{s}$
B	magnetic flux density, magnetic induction	$1 \text{ G} \rightarrow 10^{-4} \text{ T} = 10^{-4} \text{ Wb/m}^2$
H	magnetic field strength	$1 \text{ Oe} \rightarrow 10^3/(4\pi) \text{ A/m}$
m	magnetic moment	$1 \text{ erg/G} = 1 \text{ emu} \rightarrow 10^{-3} \text{ A}\cdot\text{m}^2 = 10^{-3} \text{ J/T}$
M	magnetization	$1 \text{ erg}/(\text{G}\cdot\text{cm}^3) = 1 \text{ emu/cm}^3 \rightarrow 10^3 \text{ A/m}$
$4\pi M$	magnetization	$1 \text{ G} \rightarrow 10^3/(4\pi) \text{ A/m}$
σ	mass magnetization, specific magnetization	$1 \text{ erg}/(\text{G}\cdot\text{g}) = 1 \text{ emu/g} \rightarrow 1 \text{ A}\cdot\text{m}^2/\text{kg}$
j	magnetic dipole moment	$1 \text{ erg/G} = 1 \text{ emu} \rightarrow 4\pi \times 10^{-10} \text{ Wb}\cdot\text{m}$
J	magnetic polarization	$1 \text{ erg}/(\text{G}\cdot\text{cm}^3) = 1 \text{ emu/cm}^3 \rightarrow 4\pi \times 10^{-4} \text{ T}$
χ, κ	susceptibility	$1 \rightarrow 4\pi$
χ_ρ	mass susceptibility	$1 \text{ cm}^3/\text{g} \rightarrow 4\pi \times 10^{-3} \text{ m}^3/\text{kg}$
μ	permeability	$1 \rightarrow 4\pi \times 10^{-7} \text{ H/m} = 4\pi \times 10^{-7} \text{ Wb}/(\text{A}\cdot\text{m})$
μ_r	relative permeability	$\mu \rightarrow \mu_r$
w, W	energy density	$1 \text{ erg/cm}^3 \rightarrow 10^{-1} \text{ J/m}^3$
N, D	demagnetizing factor	$1 \rightarrow 1/(4\pi)$

Gaussian units are the same as cgs emu for magnetostatics; Mx = maxwell, G = gauss, Oe = oersted; Wb = weber, V = volt, s = second, T = tesla, m = meter, A = ampere, J = joule, kg = kilogram, H = henry.